International Journal of Energetic Materials and Chemical Propulsion, 17(1):1–22 (2018)

A PREMIXED GREEN PROPELLANT CONSISTING OF N_2O AND C_2H_4: EXPERIMENTAL ANALYSIS OF QUENCHING DIAMETERS TO DESIGN FLASHBACK ARRESTERS

Lukas Werling,* Yannick Jooß, Maximilian Wenzel, Helmut Ciezki, & Stefan Schlechtriem

German Aerospace Center (DLR), Institute of Space Propulsion, Hardthausen, 74239, Germany

*Address all correspondence to: Lukas Werling, German Aerospace Center (DLR), Insitute of Space Propulsion, Hardthausen, 74239, Germany; Tel.: +49 6298 28 0; Fax: +49 6298 28 458, E-mail: Lukas.Werling@dlr.de

Original Manuscript Submitted: XX/X/2017; Final Draft Received: XX/X/2017

Across the world several so-called green propellants for in-space and orbital propulsion are investigated to replace the highly toxic hydrazine. Aside from green alternatives based on ADN and H_2O_2, the DLR Institute of Space Propulsion examines a premixed propellant consisting of dinitrogen monoxide (N_2O) and ethene (C_2H_4). The mixture called HyNOx (hydrocarbons mixed with nitrous oxide) offers high performance and low toxicity, but due to the premixed state, the danger of flame flashback across the injection system is a major issue. To avoid flashback during operation of a future engine suitable flashback arresters are needed; thus the quenching diameters and corresponding quenching Peclet numbers have to be derived. To analyze the quenching diameters, DLR uses an ignition and flashback test setup. The setup consists of two chambers separated by a fitting for capillaries which serve as flashback arresters. Capillaries with diameters between 0.1 and 0.5 mm were examined regarding their ability to quench the flame. Furthermore, one chamber can be equipped with glass windows to record high-speed videos of the flame propagation process. To obtain the critical quenching Peclet number the ignition pressure was consecutively raised until a flame flashback for a given capillary was observed. The quenching Peclet numbers were calculated according to the gas state at ignition. This resulted in critical Peclet numbers between 30 and 40. Additionally, high-speed videos were recorded to analyze the flame propagation speed during the combustion process. The average flame propagation speed was between 33 m/s for an ignition pressure of 0.49 bar and 40 m/s for an ignition pressure of 1 bar.

KEY WORDS: *green propellants, nitrous oxide fuel blends, N_2O, C_2H_4, flame flashback arresters, quenching diameters, Peclet numbers, flame propagation in closed volume, flame propagation speed*

1. INTRODUCTION

For decades, hydrazine (N_2H_4) has represented the number one rocket monopropellant for spacecraft and in-orbit propulsion. The propellant is long-term storable, has a sufficient performance

2150–766X/18/$35.00

(I_{sp}), and can easily be decomposed via catalyst. Furthermore hydrazine propulsion systems are highly reliable and offer a low system complexity.

However, despite all those advantages the use of N_2H_4 has severe drawbacks. Hydrazine is highly toxic and carcinogenic; this makes the handling, transport, and storage of the substance expensive. For example, during fueling of a satellite the workers have to use full body protection suits (so-called SCAPE suits) and subsequent to the fueling process extensive cleaning and decontamination procedures are needed.

Additionally, hydrazine was included in the "list of substances with very high concern" in Europe's REACH regulation (European Chemicals Agency, 2018) due to its high toxicity.

Due to the high toxicity, the expensive handling, and the REACH regulation, during the last decade the search for less toxic propellants as alternatives to hydrazine became more and more important. Worldwide, several so-called "green propellants" are under development, under investigation, or are already used in propulsion systems (Amrousse et al., 2017; Friedhoff et al., 2017; Gohardani et al., 2014; Gotzig et al., 2015; Gregory et al., 2012; Masse et al., 2017; Mayer et al., 2018; Sackheim and Masse, 2014).

The German Aerospace Center (DLR) in Lampoldshausen conducts research on different kinds of green propellants: e.g., ADN-based propellants, hydrogen peroxide (H_2O_2), and mixtures of hydrocarbons with nitrous oxide (HyNOx) are extensively studied (Lauck et al., 2018; Negri et al., 2018; Werling et al., 2018, 2017a; Wilhelm et al., 2017). Each of those green alternatives offer several advantages and disadvantages compared to conventional hydrazine. In this paper the focus is on a propellant based on ethene and nitrous oxide. N_2O/hydrocarbon mixtures are also-called premixed propellants: the oxidzer (N_2O) and the fuel (e.g., C_2H_2, C_2H_4, C_2H_6...) are stored premixed in one tank. Thus the high I_{sp} of a bipropellant ($\geq$ 300 s) and the simple propulsion system of a monopropellant can be combined. Furthermore due to the high vapor pressure of N_2O, self-pressurized systems could be realized.

Nevertheless, to use premixed propellants consisting of N_2O and hydrocarbons safely in future propulsion systems several challenges have to be overcome. The two main challenges of the mixture are high combustion temperatures ($\approx$ 3000 K) and the danger of flame flashback into the feeding lines and tank structure. To handle the first challenge, the high combustion temperatures, an actively cooled combustion chamber is needed. To manage the second challenge suitable flashback arresters in combination with appropriate injection systems have to be designed. By using appropriate flashback arresters a safe operation without a flame flashback and possible destruction of the whole spacecraft is achieved.

Flashback arresters can be designed by knowing the quenching diameters of the propellant mixture and via analysis of the quenching Peclet numbers. Thus the determination of the quenching diameters, the conditions under which quenching occurs, and the analysis of the corresponding quenching Peclet numbers is the scope of this paper. Additionally the flame propagation speed and flame propagation behavior of the N_2O/C_2H_4 mixture is investigated.

To analyze the quenching parameters and to investigate the ignition and flame propagation process of the gaseous N_2O/C_2H_4 propellant, DLR Lampoldshausen set up an ignition and flashback test setup. The setup consists of two closed chambers which are connected to each other by a fitting for capillaries. A previous version of this setup was already used for the investigation of porous flashback arresters (Werling et al., 2017b). In comparison to the former setup, a second window was added to the chamber where the propellant mixture is ignited. The windows allowed the observation of the ignition and flashback processes via high-speed camera. Furthermore thermocouples and pressure transducers are mounted at both chambers. These sensors are used to analyze the pressure rise during the combustion process

and to detect if a flame flashback across the capillaries from one chamber to the other occurs.

2. REACTION PROPERTIES, QUENCHING AND FLAME PROPAGATION MECHANISMS

The following section gives a short overview on the N_2O/C_2H_4 reaction properties and describes the theory behind the quenching and flame propagation processes.

2.1 Mixture and Reaction Properties

The global chemical reaction for the stoichiometric N_2O/C_2H_4 gas mixture is given by:

$$6N_2O + C_2H_4 \longrightarrow 2CO_2 + 6N_2 + 2H_2O \quad \Delta H_R^0 = -1851,4 \frac{\text{kJ}}{\text{mol}}. \tag{1}$$

The heat of reaction H_R^0 was taken from Rumble (2018). To calculate the flame properties and the laminar flame speed a reduced, optimized reaction mechanism for the N_2O/C_2H_4 combustion was used. This mechanism includes 22 species and 61 elementary reactions and is based on the GRI-Mech 3.0 (Smith et al., 2016). To match the experimental flame properties the original GRI mechanism was optimized and reduced by the Institute of Combustion Technology of DLR in Stuttgart (Kick et al., 2017; Naumann et al., 2017). The laminar flame speeds for the later analysis were calculated via the Cantera (Goodwin et al., 2016) script and the mentioned reaction mechanism.

2.2 Flame Quenching

Sir Humphry Davy was the first person who found that a flame is not able to propagate through small gaps or tubes. In the early 19th century he developed a miner's safety lamp where the flame was surrounded by a fine copper gauze and thus was not able to ignite flammable gases in coal mines (Griffiths and Barnard, 1995). Since those times flame traps and flame arresters are built the same way: they comprise an assembly of small tubes, crimped ribbons, or narrow bores to quench the flame.

Under the assumption of an ideal gas, a constant pressure across the flame front, a laminar flame structure, infinite fast heat conduction, and isothermal walls, the conditions for flame quenching can be derived (Kuo, 2005; Turns, 2000). By using the energy and mass conservation an expression for the quenching Peclet number (Pe_{cr}) depending on thermal diffusivity of the unburned gas (α_u), the laminar flame speed (S_l), and the characteristic quenching distance (d_q) is obtained:

$$\text{Pe}_{cr} = \frac{d_q \cdot S_l}{\alpha_u}. \tag{2}$$

The flame is quenched, if the present Peclet number (Pe_{quench}) is smaller or equal to the critical Peclet number Pe_{cr} [Eq. (3)].

$$\text{Pe}_{quench} \leq \text{Pe}_{cr}. \tag{3}$$

The thermal diffusivity in equation (2) can be written as the thermal conductivity of the unburned mixture (λ_u) divided by the density of the unburned mixture (ρ_u) and the heat capacity of the unburned gases ($c_{p,u}$).

$$\alpha_u = \frac{\lambda_u}{\rho_u \cdot c_{p,u}}. \tag{4}$$

Regarding the critical Peclet number (Pe_{cr}), different geometrical conditions for quenching are distinguished:

1. Head-on quenching: Here the flame moves perpendicular to a solid wall and is extinguished at a distinct distance from the wall. Typical critical Peclet numbers for head-on quenching are around 3 (Bellenoue et al., 2003; Boust et al., 2007; Poinsot et al., 1993; Wichman and Bruneaux, 1995).

2. Side wall quenching: The flame moves along a wall. In theoretical (Kármán and Millán, 1953) and experimental studies (Clendening et al., 1981; Lu et al., 1991) the Peclet number for quenching was found to be 7. In a study of propane-air mixtures Peclet numbers between 4.5 and 8.5 were found (Bellenoue et al., 2003).

3. Parallel plates quenching: For a rectangular channel Jarosiński (1983) obtained a critical Peclet number of 51 .

4. Quenching in circular tubes: A theoretical analysis of quenching in tubes was done by Spalding (1957); he derived a critical Peclet number of 60.5. According to Poinsot and Veynante (2011) quenching Peclet numbers for tubes are close to 50.

The flashback arresters used in the later described experiments were circular tubes with diameters between 0.1 and 0.5 mm. Thus the expected Peclet number for quenching should be between 50 and 60.

2.3 Flame Propagation in a Closed Vessel

During the combustion process in a closed vessel, the pressure rises continuously until the combustible mixture is consumed and enough heat is dissipated to the environment via convection or radiation. In contrast to an isobaric combustion, the flame propagation speed is thus strongly dependent on the current pressure at a certain time. Furthermore the expansion of the hot gases behind the flame front causes the flame to move several times faster than the laminar flame speed. Thus the flame propagation speed is caused by the laminar flame speed and the expansion speed of the combusted gases. Assuming energy and mass conservation and a one-dimensional isobaric, stationary flame, the flame propagation speed S_f^0 results are (Law, 2006a):

$$S_f^0 = \frac{\rho_u}{\rho_b} \cdot S_l. \tag{5}$$

During the combustion process in a closed volume, the flame propagation speed is influenced by several parameters such as increasing pressure and temperature, changes of the flame surface area, turbulence, and the combustion chamber geometry.

For the combustion process in a spherical volume or constant volume bomb, several approaches for the laminar burning velocity exist (Faghih and Chen, 2016). In general the flame propagation speed which is affected by flame stretch (S_f) can be calculated by the flame speed

without stretch (S_f^0), the flame stretch rate (κ_s), and the Markstein length (L_u) (Poinsot and Veynante, 2011) according to Eq. (6):

$$S_f = S_f^0 + L_u \cdot \kappa_s. \tag{6}$$

With evaluation and plotting the burning velocity with stretch (S_f) against the stretch rate (κ_s) and by using a linear regression to the point with zero stretch, the burning velocity without stretch can be obtained without explicit calculation of the Markstein length (Law, 2006a). Subsequent to the calculation of S_f^0 the laminar flame speed (S_l) can be calculated by Eq. (5).

During the flame propagation process in a closed volume, the initial smooth laminar flame is affected by flow and flame instabilities and undergoes the transition to a fully turbulent flame (Dorofeev, 2002; Law, 2006b; Matalon, 2009). This process can be divided into several steps (Xiao, 2016):

1. Immediately after a weak ignition the flame front is smooth and laminar; then instabilities influence the flame front and cause a wrinkled or cellular flame. Parallel with the wrinkling of the flame, the flame propagation speed rises due to a larger flame surface area.

2. The wrinkled or cellular laminar flame front is influenced by the turbulent flow field. The turbulent flow field itself is caused by an increased flow velocity of the expanding hot gases. Along with the increase in turbulence the flame surface area, grows and the flame front is affected by a further acceleration.

3. Finally, depending on the level of flame acceleration, different kinds of combustion conditions are achieved

    a. If the flame is only affected by a weak flame acceleration a slow, subsonic turbulent flame is formed.

    b. In the case of a strong flame acceleration without the occurrence of a DDT a fast supersonic turbulent flame develops.

    c. For a strong flame acceleration and the occurrence of a DDT a detonation or a quasi detonation is the final state of the combustion process.

A simple model to describe a turbulent flame front is to assume that the turbulent flame is a wrinkled or folded laminar flame (see Fig. 1) (Damköhler, 1940).

Following this definition, the laminar and turbulent flame speed and flame surface area are connected via

$$S_l \cdot A_t = S_t \cdot A_l, \tag{7}$$

so for the turbulent flame speed it follows:

$$S_t = S_l \cdot \frac{A_t}{A_l}. \tag{8}$$

According to Eq. (8) the turbulent flame speed increases proportionally to the turbulent flame surface area and the laminar flame speed. Furthermore, a general formulation for the turbulent flame speed S_t depending on laminar flame speed S_l and the root mean square of the turbulent

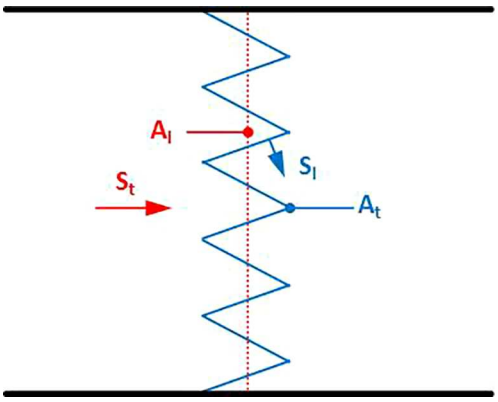

FIG. 1: Definition of turbulent flame velocity for wrinkled flamelets

velocity fluctuations u_0' can be derived from Damköhler's model (Burke et al., 2016; Peters, 1999, 2006; Zimont, 2016):

$$\frac{S_t}{S_l} = 1 + C \cdot \left(\frac{u_0'}{S_l}\right)^n, \tag{9}$$

where C is a model parameter with values on the order of unity. C depends on the ratio of the integral length scale l of the turbulence to the flame thickness [$d_f = \lambda_u/(\rho_u \cdot c_p \cdot S_l)$] while the exponent n is typically 0.7 (Peters, 2006). Equation (9) shows a limit for very low turbulence. In this case ($u_0'/S_l \ll 1$) the turbulent flame speed converges to the laminar flame speed ($S_t \approx S_l$), while for the case of growing turbulence ($u_0'/S_l \gg 1$) the turbulent flame speed increases with the turbulent velocity fluctuations until the fluctuation gets too strong and quenches the flame (Glassman et al., 2008).

3. EXPERIMENTAL SETUP

In the following section, the experimental setup, the test chambers, and the experimental procedure are described. Compared to a previous test campaign (Werling et al., 2017b) both test chambers were modified; e.g., the diameter of the flashback chamber was increased and aligned to the ignition chamber and a second window was added to the ignition chamber. In summary 129 ignition and flashback tests were conducted using the below described test configuration.

The experimental setup is located at the M11 test facility (Ciezki et al., 2017) of DLR in Lampoldshausen. It consists of three parts: a versatile feeding system for gas supply, a mixing chamber to realize premixing of N_2O and C_2H_4, and the test chambers. Figure 2 shows a simplified piping and instrumentation diagram of the test setup. On the right-hand side the gas supply, the pressure regulator, and automatic valves for filling of the premixing chamber are shown. The pressure regulators are used to adjust the pressure of the oxidizer and fuel and to achieve the wanted mixture ratio in the mixing chamber. To monitor the manually adjusted pressure and to obtain the actual pressure, two pressure sensors (P-N2O-01 and P-C2H4-01) are mounted. At the same position two type-K thermocouples (T-N2O-01 and T-C2H4-01) are located. The pressure and temperature data are used to calculate the density of the specific gas via Refprop.

Downstream of the mixing chamber an automatic valve (AV-1-Filling) for filling the test chambers is located. The test section itself consists of two chambers connected by the capillaries which serve as flashback arresters (see Fig. 3). To monitor the flame propagation and flashback

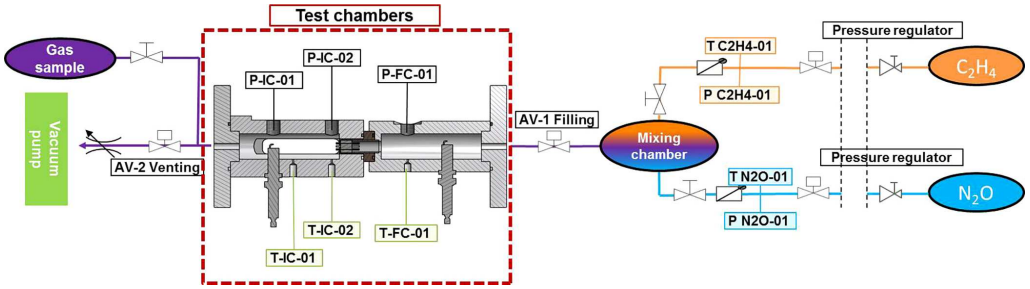

FIG. 2: Simplified P& ID of the test bench

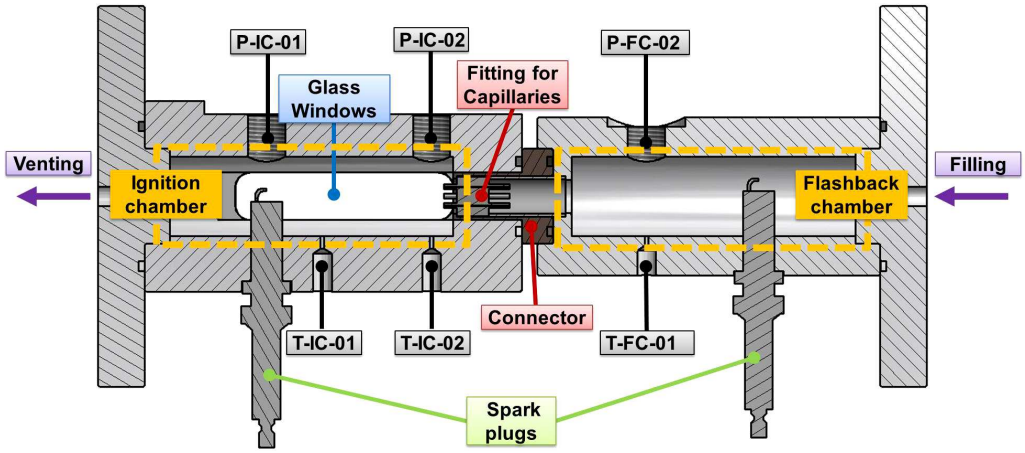

FIG. 3: Sectional drawing of the test chambers

processes, three thermocouples and three pressure transducers are attached to the test chambers. The outlet of the ignition chamber (AV-2-Venting) is connected to an interface for gas sampling and a vacuum pump. The vacuum pump is used to evacuate the test chambers prior to each test run and to remove the combusted gases subsequent to each test run.

3.1 Test Chambers

A sectional drawing of the test chambers is given in Fig. 3.

The setup consists of an ignition and a flashback chamber. During most of the test runs, the gaseous N_2O/C_2H_4 mixture was ignited at the spark plug of the ignition chamber (left side). During those test runs, the ignition and flame propagation process could be observed via a high-speed camera (Photron Fastcam SA 1.1) through two glass windows. The glass windows withstood ignition pressures of up to 2.2 bar. For higher ignition pressures steel plates instead of glass windows were used. To assure a sufficient resolution of the flame propagation, the camera's frame rate was between 67,500 and 93,000 frames per second. Additionally, in several test runs the mixture was ignited at the flashback chamber to film the flame behavior at the outlet of the capillaries when a flashback occurred. During the flame propagation the pressure was monitored via two pressure transducers (P-IC-01 and P-IC-02, manufacturer: STS, Type: TM-600 bar) in the ignition chamber and one transducer in the flashback chamber (P-FC-01, manufacturer:

STS, Type: TM-600 bar). The sensor in the flashback chamber was used to detect if a flame flashback occurred or not. Additionally two thermocouples (type-K, sheath thermocouple with 1 mm diameter) in the ignition chamber and one thermocouple (type-K, sheath thermocouple with 0.5 mm diameter) in the flashback chamber were used to determine if the flame passed the capillaries. The data acquisition rate for the pressure transducers were 50 kHz, while the thermocouples' data was acquired with 100 Hz. The inner diameter of each chamber is 25 mm and the cylindrical volume has a length of 91 mm. Both spark plugs are located 60 mm from the connecting element, which is in between both chambers.

Capillaries with diameters ranging from 0.1 to 0.5 mm were used. The diameter was chosen due to two reasons: First, the experimental safety gap of N_2O/C_2H_4 at 1 bar is 0.26 mm (Meye et al., 2012). The authors wanted to evaluate the quenching diameters below and above this margin. Second, in a prior test campaign porous materials with pore diameters smaller than 0.5 mm were used (Werling et al., 2017b). By choosing a comparable diameter (around and smaller than 0.5 mm), the quenching ability of the capillaries could be comparable to quenching behavior of the previously tested porous materials.

The length of all capillaries used was 21 mm; this dimension was chosen according to the length of previously tested porous materials. Furthermore this length assured that the edge (depending on ignition position, the entrance, or exit) of the capillaries was visible through the glass windows, so a flame entering or exiting the capillaries could be observed directly via high-speed video. Additionally, due to the size and geometry of the test setup, shorter capillaries were difficult to mount in the capillary fitting.

One holder/fitting for the capillaries took four of the microtubes to achieve a sufficiently large gas flow during filling of the test section (see Fig. 4). The maximum number of capillaries was limited to four due to the available space in the capillaries' fitting.

The fitting for the capillaries was mounted flush to the left side of the connector; thus the capillaries extend 2–3 mm into the ignition chamber.

Figure 4 shows some of the tested microtubes/capillaries.

FIG. 4: Fittings with a selection of the tested capillaries

3.2 Experimental Procedure

The test preparation and conduction was done according to Figs. 5(a) and 5(b).

At the beginning of each test campaign, the whole setup was evacuated via vacuum pump. After evacuation the mixing chamber was pressurized with C_2H_4 to approximately 6 bar. When the mixing vessel was filled with ethene, the pressure and temperature of the gas in the mixing chamber was taken to determine the density of ethene via the Refprop database (Lemmon et al., 2013). Subsequently the needed pressure for a near-stoichiometric mixture of N_2O/C_2H_4 was also calculated via Refprop. This was done under the assumption of ideal gas mixing and an identical mixing volume for N_2O and C_2H_4.

After pressurizing the mixing chamber with N_2O, all valves were closed and the gases were allowed to rest for 5 min to assure proper mixing.

Subsequently, the test chambers (Fig. 3) were filled with propellant mixture and a gas sample was taken to analyze the achieved mixture ratio via gas chromatography. Afterwards the test setup was ready for the ignition and flashback tests.

All tests were done according to Fig. 5(b). Prior to ignition the chambers were filled with a gaseous dinitrogen monoxide/ethene mixture. The pressure was adjusted via venting of the chambers with the vacuum pump. When the desired pressure was reached, the venting valve was closed, the gases were allowed to rest, and the automatic test sequence was started. Then the measurement and control systems acquired the temperature and pressure data, and triggered the high-speed camera and the spark plug. After ignition of the N_2O/C_2H_4 mixture, the venting valve was used again to remove the combusted gases and evacuate the chambers. When the chambers were evacuated (pressure below 20 mbar), the setup was ready for the next ignition test.

To determine the maximum ignition pressure where the capillaries were still able to quench the flame, the pressure was raised gradually from test to test until a flame flashback occurred. When a pressure level was reached where the flame passed the capillaries, the pressure was reduced again, until the flame was not able to propagate through the capillaries anymore. The conditions at the highest ignition pressure where no flashback occurred were used to calculate the critical Peclet numbers.

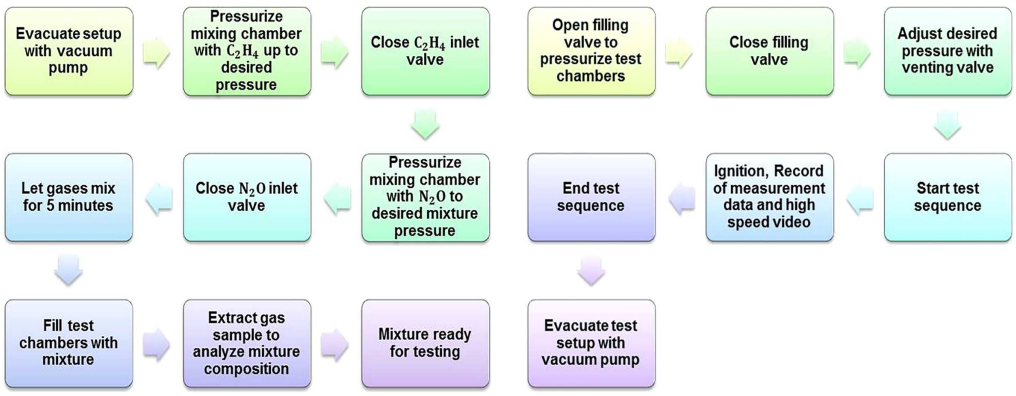

FIG. 5: Test preparation and conduction; (a) test preparation flow chart, (b) test conduction flow chart

3.3 Test Conditions and Data Acquisition

All tests were conducted according to the above described experimental procedure [Fig. 5(b)] using the test chambers (Fig. 3). However, during the experiments the test conditions changed due to different ignition pressures and different positions of the ignition source (left or right spark plug in Fig. 3). In summary tests were conducted under the following conditions:

1. Ignition via spark plug in the ignition chamber (left chamber in Fig. 3) up to a maximum pressure of 2.2 bar. For these tests glass windows were used; the windows limited the maximum ignition pressure. During these tests the following data were collected:
    a. High-speed videos for determination of the flame propagation speed
    b. Pressure and temperature in the ignition and flashback chamber to determine if a flame flashback across the capillaries occurred.
2. Ignition via spark plug in the ignition chamber (left chamber in Fig. 3) up to a maximum pressure of 4.65 bar. To achieve higher pressure levels, steel plates instead of glass windows were used. The data collected here were:
    a. Pressure and temperature in the ignition and flashback chamber to determine if a flame flashback across the capillaries occurred.
3. Ignition via spark plug in the flashback chamber (right chamber in Fig. 3) up to a maximum pressure of 2.2 bar. Here the following data were collected:
    a. High-speed videos for analysis of the flame propagation after passing the capillaries. For those tests videos were only available if a flashback from the flashback chamber to the ignition chamber occurred, because the flashback chamber is not equipped with a window (see Fig. 3)
    b. Pressure and temperature in the ignition and flashback chamber.

4. EXPERIMENTAL RESULTS AND DISCUSSION

During the test campaign, pressure and temperature data as well as high-speed videos were recorded. The pressure and temperature data were used to detect whether the flame passed the capillaries and a flashback occurred. Furthermore if the ignition was initiated at the ignition chamber, the high-speed videos were used to determine the flame propagation speed. Otherwise if the ignition was initiated at the spark plug of the flashback chamber, the high-speed videos were used to record the flame behavior after a flame flashback across the capillaries.

4.1 High-Speed Videos of Flame Propagation

Figure 6 shows typical frames of a high-speed video during the flame propagation process in the ignition chamber.

During the combustion process, different phases of the flame propagation process can be distinguished:

1. After ignition a nearly spherical flame forms around the spark plug. The flame propagates outwards until the flow field interacts with the walls of the cylindrical combustion chamber (frames 1–4).

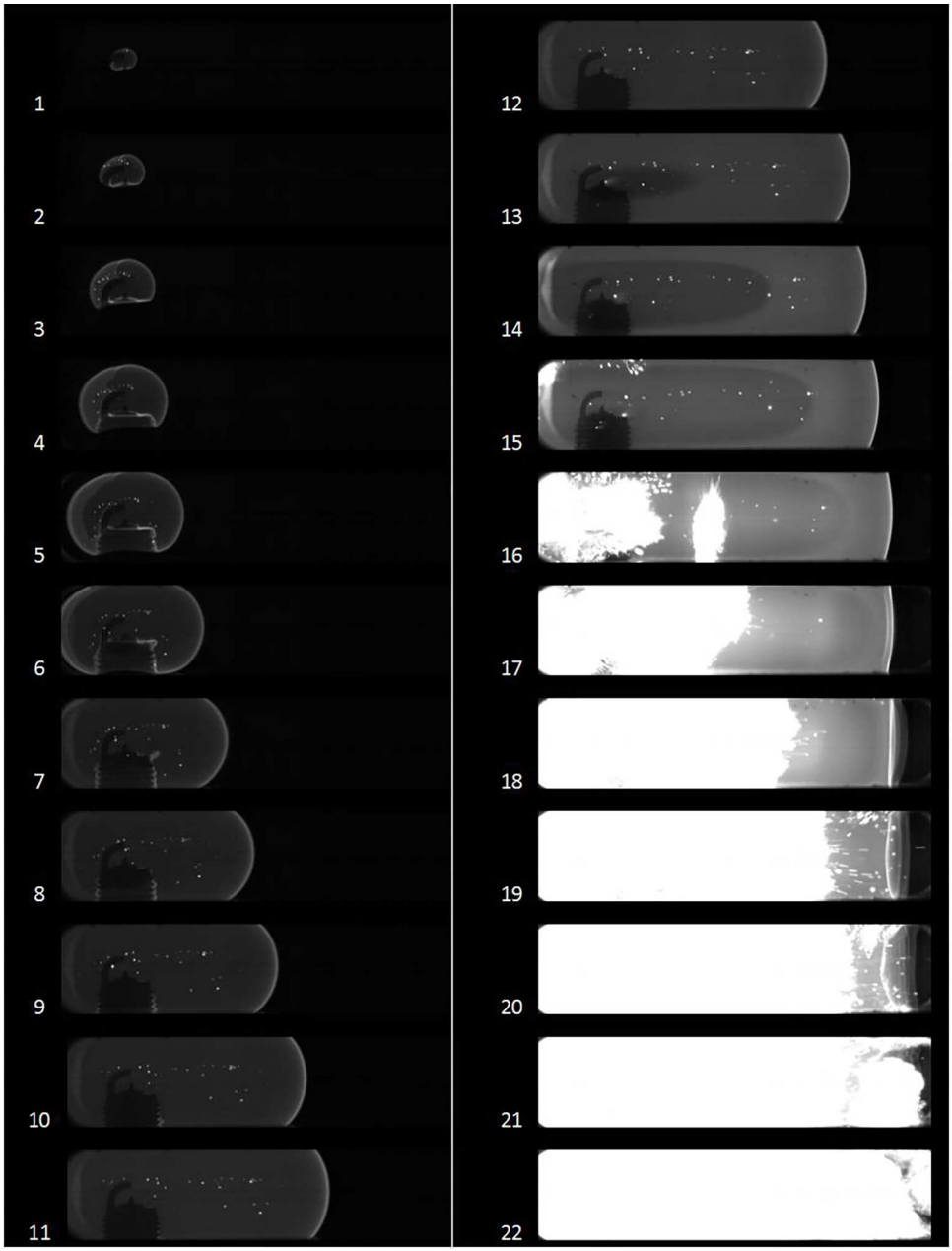

FIG. 6: Flame propagation in the ignition chamber: time difference between two frames is 87 μs; absolute pressure at ignition = 0.61 bar; temperature at ignition = 292 K; fuel-to-oxidizer equivalence ratio (ϕ) = 1.2

2. The flame front approaches the chamber walls (the walls are not visible on the high-speed images) and a “finger-like” flame is formed. The flame accelerates in the axial direction (frames 5–12).

3. The flame front is quenched at the walls and at the windows; thus the flames' surface area is reduced and the flame acceleration stops. Quenching at the windows can be identified via a slight dark shadow. This shadow begins growing at the spark plug in frame 13 and is visible until frame 17. The bright jets of hot gases at the left and bottom in frame 16 are caused by turbulent and fast combustion of gases in the venting line, respectively, in a thermocouple fitting. When the flame front enters these constrictions it is accelerated, instabilities are formed, and the flame front becomes turbulent. The turbulent flame causes a higher consumption rate of the unburned gas which leads to a local pressure rise. Due to the local pressure rise the reacting gases expand into the ignition chamber.

4. The flame front slows down in the axial direction, caused by the interaction of the flow field with the chamber wall (frame 17). The shape of the flame changes from the "finger-like" convex shape to a nearly vertical shape (frame 18) and finally an inversion of the flame occurs (frame 19). During the inversion, the flame is presumably affected by pressure fluctuations which cause instabilities and finally lead to a turbulent flame (frames 21 and 22). If the axial length of the ignition chamber were sufficiently large, the inversion might lead to a tulip flame. A comprehensive description of the flame propagation processes in ducts and the tulip flame phenomena can be found in Dunn-Rankin and Sawyer (1998), Ponizy et al. (2014), and Xiao et al. (2015)

The high-speed videos of the flame propagation were used to analyze the development of the flame velocity during a single combustion test. Additionally, tests with different ignition pressures were compared to investigate the dependency of the average flame speed on the ignition pressure.

4.2 Flame Propagation Speed

The flame propagation speed was determined by processing the high-speed videos via Matlab image processing script. The Matlab script detects the flame front position in the current frame at a horizontal line, starting at the position where the spark occurred. To calculate the velocity between two frames, the axial displacement of the flame front was divided by the time between the two frames. Due to reflections in the videos, glowing particles, and discrete velocity values caused by the video resolution, the automated velocity examination needed manual corrections.

Additionally, the average flame speed was determined by measuring the time span the flame tip needed to reach a fixed position at 43 mm distance to the spark plug. At this location (43 mm) the flame front was clearly visible up to ignition pressures of 1.1 bar. Thus disturbances by reflections or turbulences at the end of the chamber could be avoided. To obtain the average flame speed the distance was divided by the time the flame tip needed to reach this position.

Figure 7(a) shows the typical velocity profile during a single ignition test. The flame speed was evaluated at three pixel lines: at the line where the spark was first detected, one pixel row below, and one row above this line. During the combustion process different areas of the flame speed can be distinguished.

Shortly after ignition the flame propagates spherically and the flame speed rises with increasing flame surface. Subsequently to the spherical propagation the flame approaches the chamber walls. Near the walls the flow slows down, while the flame surface area still grows. The burned gases behind the flame front at the walls cannot expand into the direction of the walls anymore, so the gases are deflected in the axial direction. This causes a further acceleration of the flame

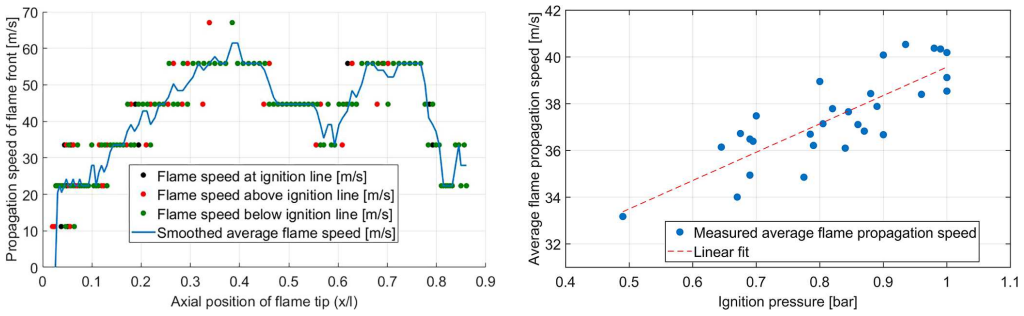

(a) (b)

FIG. 7: Flame propagation speeds. (a) Flame propagation speed during a test run: ignition pressure 0.79 bar; ignition temperature 23°C. Current position of flame tip (x) divided by the distance between spark plug and capillaries (l). (b) Average flame propagation speed for tests with ignition pressures between 0.5 and 1 bar

front. A first maximum of the flame speed occurs at x/l = 0.4. After this point the flame is influenced by two opposing effects. On the one hand, the flame surface still grows, which increases the flame propagation speed. On the other hand, the laminar flame speed decreases due to the rising pressure. In summary this should led to a nearly constant flame propagation speed. However, a strong drop of the flame speed (x/l = 0.6) followed by a rise to the former value (x/l = 0.7) of 60 m/s is visible. The authors assume that this decline and the following rise in flame propagation speed is caused by the interaction of the flame front and flow with a pressure wave reflected by the right chamber wall. The pressure data show several oscillations inside the chamber, but due to the high frequency and low amplitude of the oscillations the effect cannot be investigated in detail. After the fall and rise of the flame propagation velocity, the flame approaches the right wall and slows down.

Figure 7(b) shows the average flame propagation speed for ignition pressures from 0.49 to 1.0 bar. The evaluation of the flame speed for ignition pressures higher than 1.1 bar was difficult due to overexposure of the camera and bright reflections. The variations in the experimentally obtained values are most likely caused by slight temperature and mixture ratio variations as well as errors during evaluation. Nevertheless, the ignition pressure and the average flame speed seem to follow a linear correlation. For an ignition pressure of 0.49 bar the average flame propagation speed is approximately 33 m/s, while for an ignition pressure of 1.0 bar the average speed increases to 40 m/s.

According to Eq. (5) the flame propagation speed S_f^0 depends on the ratio of the unburned gas density to the burned gas density and the laminar flame speed. Calculations with NASA CEA (Gordon and McBride, 1996) for the burned to unburned density ratio show an increase in the density ratio with rising pressure, while laminar flame speed calculation with Cantera (Goodwin et al., 2016) shows a decreases of the laminar flame speed with increasing pressure. However, combining both effects in Eq. (5) leads to a slight drop of the theoretical flame propagation speed with increasing pressure.

In the experimental data the opposite trend is found; thus other factors influencing the flame seem to increase the flame propagation speed. Due to Eq. (8) and (9) an increase in turbulence, respectively, flame surface area leads to a higher flame propagation speed. The comparison of the high-speed images of a test with an ignition pressure of 0.59 bar [Fig. 8(a)] to a test with

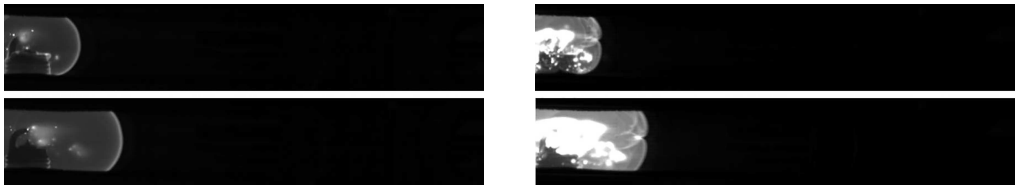

(a) (b)

FIG. 8: Flame shapes for different ignition pressures: (a) flame shape at an ignition pressure of 0.59 bar; (b) flame shape at an ignition pressue of 2.12 bar

a pressure of 2.12 bar [Fig. 8(b)] shows that the flame with the higher pressure is affected by several instabilities and a cellular flame is formed. Therefore it is assumed that instabilities are causing the increase of the average flame speed for higher pressure levels. The effect of rising flame speed with pressure due to instabilities is also mentioned by Law (2006a).

4.3 Pressure and Temperature Data

Typical pressure and temperature data for a test without flashback are given in Figs. 9(a) and 9(b).

Figure 9(a) shows the pressure rise during the ignition and flame propagation process in the ignition chamber (sensor P-IC-01 and P-IC-02). An exponential increase in pressure is visible during the combustion process. The peak value of the pressure at P-IC-01 and P-IC-02 (17 bar) is approximately 21 times larger than the ignition pressure (0.79 bar). In the flashback chamber (sensor P-FC-01) no pressure rise is recorded; however, some oscillations due to vibrations of the test setup are visible.

In Fig. 9(b) the corresponding temperature data are shown. Due to the comparatively low response time of the type-K thermocouples, the temperature maximum in the ignition chamber (T-IC-01, T-IC-02) is measured 0.25–0.5 s after the pressure sensors show the peak value. As for the pressure data no sharp temperature rise is measurable in the flashback chamber; thus no flashback occurred.

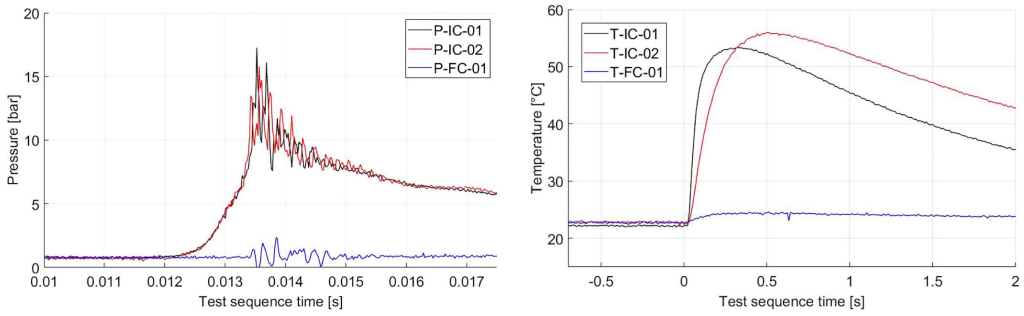

(a) (b)

FIG. 9: Pressure and temperature data without flashback. (a)Pressure data without flashback: ignition pressure 0.79 bar; ignition temperature 23°C; 0.4 mm capillaries. (b)Temperature data without flashback: ignition pressure 0.79 bar; ignition temperature 23°C; 0.4mm capillaries

In contrast to Figs. 9(a) and 9(b), Figs. 10(a) and 10(b) give the pressure and temperature profiles for a test where the flame was able to pass the capillaries.

Figure 10(a) shows a sharp pressure peak in the flashback chamber (P-IC-01), approximately half a millisecond after the pressure maximum is reach in the ignition chamber (P-IC-01, P-IC-02). According to the pressure profile, the temperature data [Fig. 10(b)] in the flashback chamber (T-FC-01) also show a sharp peak. The higher peak value and quicker response time of T-FC-01 are caused by the smaller diameter of this thermocouple. While T-IC-01 and T-IC-02 have a diameter of 1 mm, the diameter of T-FC-01 is 0.5 mm.

4.4 Quenching Peclet Numbers

During a test series for a given capillary with a specific diameter the ignition pressure was raised step by step, until a flame flashback from the ignition chamber to the flashback chamber was detected. When a pressure level was reached where the flame was able to pass the capillaries, the ignition pressure was reduced again, until the flame was not able to pass the capillaries anymore. The highest pressure at which the flame was still quenched was then taken to calculate the critical quenching Peclet number via Eq. (2). The heat conductivity λ_u, the density ρ_u, and the heat capacity $c_{p,u}$, respectively, the thermal diffusivity α_u were taken from the Refprop database (Lemmon et al., 2013). Due to reflections, bright flashes, and overexposure of the high-speed images near the entrance of the capillaries, it was impossible to determine the exact moment, and with this the exact pressure, when the flame entered the capillaries. Thus for calculation of the Peclet numbers the pressure and temperature at ignition were taken into account.

This approach leads to deviations in the calculated critical Peclet number: During the flame propagation process the laminar flame speed slightly decreases, while the density of the unburned gas strongly increases with rising pressure. The thermal conductivity and the heat capacity of the fresh gases nearly keep the same value for a specific pressure range. Thus the rising pressure in the chamber continuously reduces the quenching diameter, if a constant critical Peclet number is assumed [Eq. 2]. When the flame enters the capillaries the pressure in the ignition chamber is significantly larger than at ignition [see, e.g., Fig. 10(a)]. Thus, related to the conditions at ignition, a smaller diameter is needed to quench the flame. If the gas properties at ignition are

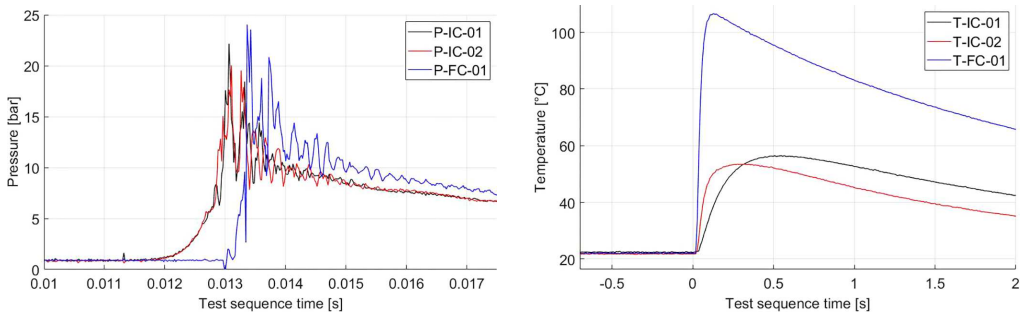

(a) (b)

FIG. 10: Pressure and temperature data with flashback. (a) Pressure data with flashback: ignition pressure 0.89 bar; ignition temperature 23°C; 0.4 mm capillaries. (b) Temperature data with flashback: ignition pressure 0.89 bar; ignition temperature 23°C; 0.4 mm capillaries

now taken into account and the quenching diameter is determined at a higher pressure level, a smaller critical Peclet number results [see Eq. (2)].

Finally the above- mentioned approach leads to a lower Peclet number compared to the theoretical values.

Table 1 gives the maximum pressure at which the flame was quenched, the minimum pressure where the flame was able to pass the capillaries, plus the corresponding temperature and mixture ratio. The mixture ratio for the respective test series was analyzed via gas chromatography.

Figure 11 shows the calculated critical Peclet numbers for the tested capillaries. In contrast to a theoretical value of $\mathrm{Pe}_{cr} \approx 50$–$60$ the critical Peclet numbers for the conducted experiments are between 30 and 40. For Peclet numbers smaller than the critical value the flame is quenched; for numbers larger than the critical value the flame can pass the capillary.

To derive the error bars in Fig. 11, the deviations of the pressure and temperature sensors as well as the tolerances of the capillaries were taken into account. The error of pressure and temperature sensors influence the Peclet number via the laminar flame speed S_l and the thermal diffusivity α_u. Compared to the deviations of the capillary diameter caused by manufacturing tolerances, the error of the pressure and temperature sensors are small. A tolerance of ± 0.025 mm on the capillary diameter causes the major part of the shown error bars.

In addition Fig. 11 shows slight differences between the critical Peclet numbers. The critical Peclet number seems to drop from 40 for the 0.5 mm capillary to 30 for the 0.3 mm capillary. Furthermore, for diameters smaller than 0.3 mm, the critical Peclet number seems to rise again. A major factor influencing the rise of the critical Peclet number for diameters of 0.2 and 0.1 mm

TABLE 1: Capillary diameters and conditions at ignition for the determination of the critical Peclet numbers

Capillary diameter (mm)	Length (mm)	Max. pressure for quenching (bar)	Min. pressure at flashback (bar)	Temperature (K)	Stoichiometric mixture ratio ϕ (-)
0.5	21	0.69	0.7	287	1.1
0.4	21	0.76	0.82	295	1.1
0.3	21	0.96	0.98	295	1.1
0.2	21	1.55	1.60	288	1.1
0.1	21	4.55	4.65	291	1.1

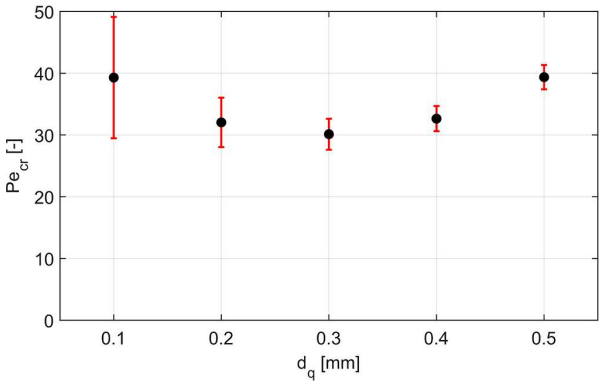

FIG. 11: Critical Peclet numbers for the tested capillary tubes

might be caused by the nonoccurrence of a reignition after the flame passed the capillary. During experiments where the spark plug in the flashback chamber was used to initiate the flame, several videos were recorded where the flame passed the capillaries but did not light the unburned gas in the ignition chamber. It is assumed that during those "backwards tests" the amount of energy escaping the capillaries was dissipated strongly in the ignition chamber and the heat was not sufficient to light the fresh mixture.

Figure 12(a) shows a flame immediately igniting the mixture in the ignition chamber during one of the "backwards tests," whereas Fig. 12(b) demonstrates the process where a flame passed the capillaries but an ignition of the unburned N_2O/C_2H_4 mixture did not occur.

Furthermore Fig. 12(a) shows that a highly turbulent flame is emerging when the flame passed the capillaries. In this case the flame propagation speeds are on the order of the sonic velocity of the unburned mixture (approx. 270 m/s).

5. SUMMARY AND CONCLUSIONS

The present paper summarizes the results of flame propagation and quenching experiments with a near-stoichiometric N_2O/C_2H_4 mixture. The nitrous oxide/ethene mixture is considered as a premixed green propellant for space propulsion applications. During DLRs research activities with an experimental rocket combustion chamber, flame flashback across the injection system

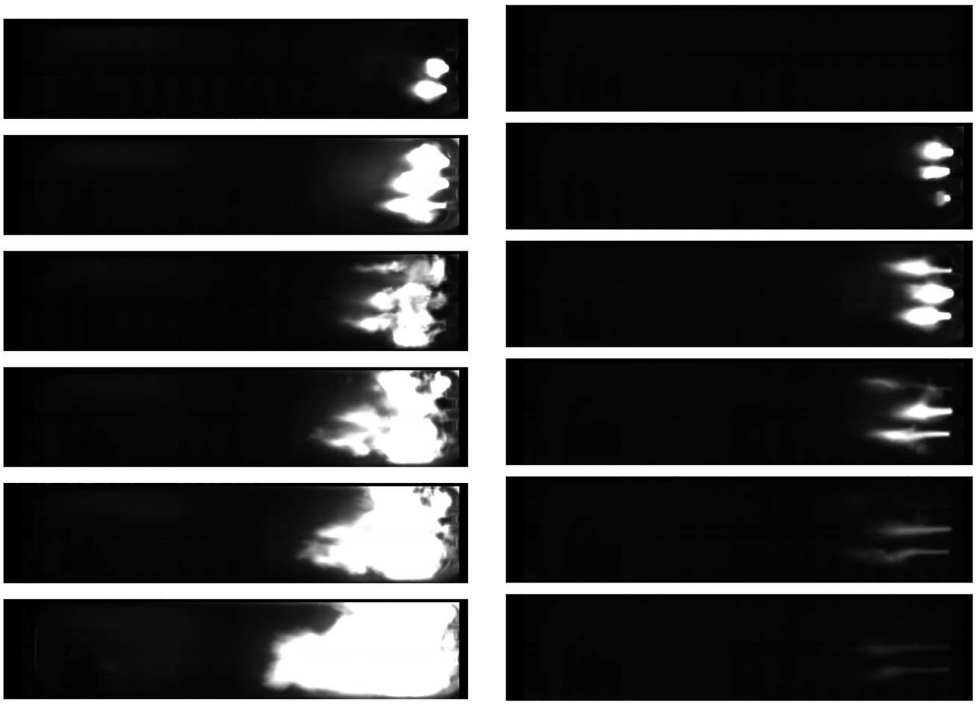

(a) (b)

FIG. 12: Flame flashback with and without ignition of the fresh gases. (a) Flame flashback with immediate ignition of the unburned mixture: ignition pressure 1.31 bar; time between frames 10 μs. (b) Flame flashback without ignition of the unburned mixture: ignition pressure 0.69 bar; time between frames 10 μs.

was found to be a major challenge. Thus, to safely use the propellant in a future propulsion system, the feeding lines of the engine have to be equipped with a suitable flashback arrester.

To analyze the flame propagation and quenching behavior of the premixed gases, an experimental setup was built. The setup consists of two chambers—a so-called ignition and a flashback chamber. Each chamber is equipped with a conventional car spark plug to initiate the ignition of the N_2O/C_2H_4 mixture. Furthermore at the ignition chamber two glass windows are installed to investigate the flame propagation process via high-speed video. Both chambers are connected by small capillaries/microtubes which serve as flashback arresters. The diameters of the tested capillaries range from 0.1 to 0.5 mm.

In several test series two parameters were investigated in detail: first, the flame propagation speed depending on the pressure at ignition. Second, the critical quenching Peclet numbers for the given pressure and capillary diameter.

Concerning the flame propagation speed the following results were obtained:

1. The average flame propagation speed measured between the spark plug and a fixed position in front of the capillaries rises nearly linear from 33 m/s for an ignition pressure of 0.49 bar to 40 m/s for 1.0 bar.

2. The rise in average flame propagation speed with increasing pressure is most likely caused by larger instabilities at the laminar flame front. These instabilities induce a cellular structure of the laminar flame.

3. The flame propagation velocity during a test run can be divided into the following sections:

    a. Acceleration of a spherical laminar flame around the spark plug.

    b. Further acceleration of the finger-like flame in the axial direction after the flame approached the walls.

    c. Deceleration followed by an acceleration of the flame front to the former velocity; this is probably caused by an interaction of the flame front with a reflected pressure wave from the chamber walls.

    d. Deceleration of the flame front caused by a slowing down of the main flow field in front of the capillaries.

Regarding the quenching experiments and the critical Peclet numbers, the following was observed:

1. The critical Peclet numbers for quenching are in the range of 30–40 for the investigated capillaries with diameters ranging from 0.1 to 0.5 mm.

2. The Peclet numbers are smaller than the theoretical values of 50–60. This is caused by the calculation method: while ideally the gas state at the inlet of the flame arrester should be taken into account, the setup and experiments only allowed the calculation with the initial values. With rising pressure during the combustion process, the quenching diameter decreases, which finally leads to the smaller calculated Peclet numbers.

3. In a small pressure range the flame can pass the capillaries but the unburned gas in the other chamber will not light. If very small amounts of burning gas are passing the capillaries an emission of light is visible, but a reignition of the fresh gases does not take

place. This effect increases with smaller diameters or smaller cross-sectional areas of the capillaries. The smaller the diameter the smaller the amount of energy released into the unburned mixture. A critical amount of unburned gas needs to be heated by the flame to continue the flame propagation.

4. After a flame flashback occurred, the flame is highly turbulent and moves with a velocity near the sonic velocity of the unburned mixture (approx. 270 m/s).

ACKNOWLEDGMENTS

The authors would like to acknowledge the help of the M11 test bench team for their support in preparing and conducting the experiments. Furthermore, great thanks go to Torsten Methling and Clemens Naumann from DLR Institute of Combustion Technology for their work regarding the N_2O and C_2H_4 reaction mechanism. Additionally, the support of Robert Stützer for providing a spare high-speed camera is greatly acknowledged.

REFERENCES

Amrousse, R., Katsumi, T., Azuma, N., and Hori, K., (2017) Hydroxylammonium Nitrate (Han)-Based Green Propellant as Alternative Energy Resource for Potential Hydrazine Substitution: From Lab Scale to Pilot Plant Scale-Up, *Combust. Flame*, **176**(1), pp. 334–348.

Bellenoue, M., Kageyama, T., Labuda, S.A., and Sotton, J., (2003) Direct Measurement of Laminar Flame Quenching Distance in a Closed Vessel, *Exper. Thermal Fluid Sci.*, **27**(3), pp. 323–331.

Boust, B., Sotton, J., Labuda, S.A., and Bellenoue, M., (2007) A Thermal Formulation for Single-Wall Quenching of Transient Laminar Flames, *Combust. Flame*, **149**(3), pp. 286–294.

Burke, E.M., Güthe, F., and Monaghan, R.F.D., (2016) A Comparison of Turbulent Flame Speed Correlations for Hydrocarbon Fuels at Elevated Pressures, in *Proc. of the ASME Turbo Expo: Turbine Technical Conference and Exposition - 2016*, The American Society of Mechanical Engineers, New York, N.Y.

Ciezki, H.K., Werling, L., Negri, M., Strauss, F., Kobald, M., Kirchberger, C., Freudenmann, D., Wilhelm, M., and Petrarolo, A., (2017) 50 Years of Test Complex M11 in Lampoldshausen - Research on Space Propulsion Systems for Tomorrow, in *Proc. of 7th European Conf. for Aeronautics and Space Sciences (EUCASS), Milano, Italy, July 03–06, 2017.*

Clendening, C.W., Shackleford, W., and Hilyard, R., (1981) Raman Scattering Measurements in a Side-Wall Quench Layer, *Symp. (Int.) Combust.*, **18**(1), pp. 1583–1590.

Damköhler, G., (1940) Der Einfluss der Turbulenz auf die Flammengeschwindigkeit in Gasgemischen, *Z. Elektrochem. Angew. Phys. Chem.,*, **46**(11), pp. 601–652.

Dorofeev, S.B., (2002) Flame Acceleration and Ddt in Gas Explosions, *J. Phys. IV (Proc.)*, **12**(7), pp. 3–10.

Dunn-Rankin, D. and Sawyer, R.F., (1998) Tulip Flames: Changes in Shape of Premixed Flames Propagating in Closed Tubes, *Exper. Fluids*, **24**(2), pp. 130–140.

European Chemicals Agency, (26.06.2018) Candidate List of Substances of Very High Concern for Authorisation: Published in Accordance with Article 59(10) of the REACH Regulation, available from echa.europa.eu/candidate-list-table.

Faghih, M. and Chen, Z., (2016) The Constant-Volume Propagating Spherical Flame Method for Laminar Flame Speed Measurement, *Sci. Bull.*, **61**(16), pp. 1296–1310.

Friedhoff, P., Hawkins, A., Carrico, J., Dyer, J., and Kjell, A., (2017) In-Orbit Operation and Performance of Ammonium Dinitramide (ADN) Based High Performance Green Propulsion (HPGP) Systems, in *53rd AIAA/SAE/ASEE Joint Propulsion Conf., AIAA Propulsion and Energy Forum.*

Glassman, I., Glumac, N., and Yetter, R.A., (2008) *Combustion*, 4 ed., Amsterdam, Netherlands: Elsevier and Academic Press.

Gohardani, A.S., Stanojev, J., Demairé, A., Anflo, K., Persson, M., Wingborg, N., and Nilsson, C., (2014) Green Space Propulsion: Opportunities and Prospects, *Prog. Aerosp. Sci.*, **71**(1), pp. 128–149.

Goodwin, D.G., Moffat, H.K., and Speth, R.L., (2016) CANTERA, Version 2.2.1: An Object-Oriented Software Toolkit for Chemical Kinetics, Thermodynamics, and Transport Processes.

Gordon, S. and McBride, B., (1996) Computer Program for Calculation of Complex Chemical Equilibrium Compositions and Applications: NASA Reference Publication 1311: I. Analysis.

Gotzig, U., Kraus, S., Welberg, D., Fiot, D., Michaud, P., Desaguier, C., Casu, S., Geiger, B., and Kiemel, R., (2015) Development and Test of a 3D printed Hydrogen Peroxide Flight Control Thruster, in *Proc. of 51st AIAA/SAE/ASEE Joint Propulsion Conf.*, Orlando, FL, USA,July 27–29, 2015.

Gregory, M., Vozoff, M., and Rishikof, B., (2012) NOFBX: a New-Nontoxic Green Propulsion Technology with High Performance and Low Cost, in *Proc. of 63rd Int. Astronautical Congress*, Naples, Italy, October 1–5, 2012.

Griffiths, J.F. and Barnard, J.A., (1995) *Flame and Combustion*, 3rd. ed., London, UK: Blackie Acad. & Professional.

Jarosiński, J., (1983) Flame Quenching by a Cold Wall, *Combust. Flame*, **50**(1), pp. 167–175.

Kármán, T.v. and Millán, G., (1953) Thermal Theory of a Laminar Flame Front Near a Cold Wall, *Symp. (Int.) Combust.*, **4**(1), pp. 173–177.

Kick, T., Starke, J.H., and Naumann, C., (2017) Green Propellant Substituting Hydrazine: Investigation of Ignition Delay Time and Laminar Flame Speed of Ethene/Dinitrogen Oxide Mixtures, in *Proc. of 8th European Combustion Meeting*.

Kuo, K.K., (2005) *Principles of Combustion*, 2nd ed., Hoboken, NJ: Wiley.

Lauck, F., Negri, M., Wilhelm, M., Freudenmann, D., Schlechtriem, S., Wurdak, M., and Gotzig, U., (2018) Test Bench Preparation and Hot Firing Tests of a 1n Hydrogen Peroxide Monpropellant Thruster, in *Proc. of Space Propulsion Conf.* Sevilla, Spain, 2018.

Law, C.K., (2006a) *Combustion Physics*, Cambridge and New York: Cambridge University Press.

Law, C.K., (2006b) Propagation, Structure and Limit Phenomena of Laminar Flames at Elevated Pressures, *Combust. Sci. Technol.*, **178**(1-3), pp. 335–360.

Lemmon, E.W., Bell, I.H., Huber, M.L., and McLinden, M.O., (2013) NIST Reference Fluid Thermodynamic and Transport Properties Database: Version 9.1, NIST Standard Reference Database 23.

Lu, J.H., Ezekoye, O., Greif, R., and Sawyer, R.F., (1991) Unsteady Heat Transfer During Side Wall Quenching of a Laminar Flame, *Symp. (Int.) Combustl*, **23**(1), pp. 441–446.

Masse, R., Allen, M., Spores, R., and Driscoll, E.A., (2017) AF-M315E Propulsion System Advances and Improvements, in *Proc. of 52nd AIAA/SAE/ASME Joint Propulsion Conf.*, Salt Lake City, UT, USA, July 25–27, 2017.

Matalon, M., (2009) Flame Dynamics, *Proc. Combust. Inst.*, **32**(1), pp. 57–82.

Mayer, A.E., Wieling, W., Watts, A., Poucet, M., Waugh, I., Macfarlane, J., and Valencia-Bel, F., (2018) European Fuel Blend Development for In-Space Propulsion, in *Proc. of Space Propulsion Conf.*, Sevilla, Spain, 2018.

Meye, T., Brandes, E., Höding, M., and Busse, S., (2012) Safety Characteristics at Non-Atmospheric Conditions—Oxidizers Other than Air, in *Proc. of 9th ISPHMIE*, Cracow, Poland, 2012.

Naumann, C., Kick, T., Methling, T., Braun-Unkhoff, M., and Riedel, U., (2017) Ethene/Dinitrogen Oxide—A Green Propellant to Substitute Hydrazine: Investigation on its Ignition Delay Time and Laminar Flame Speed, in *Proc. of 26th Int. Colloquium on the Dynamics of Explosions and Reactive Systems (ICDERS)*.

Negri, M., Wilhelm, M., Hendrich, C., Wingborg, N., Gediminas, L., Adelöw, L., Maleix, C., Chabernaud, P., Brahmi, R., Beauchet, R., Batonneau, Y., Kappenstein, C., Koopmans, R.J., Schuh, S., Bartok, T., Scharlemann, C., Gotzig, U., and Schwentenwein, M., (2018) New Technologies for Ammonium Dinitramide Based Monopropellant Thrusters—The Project RHEFORM, *Acta Astronaut.*, **143**(1), pp. 105–117.

Peters, N., (1999) The Turbulent Burning Velocity for Large-Scale and Small-Scale Turbulence, *J. Fluid Mech.*, **384**(1), pp. 107–132.

Peters, N., (2006) *Turbulent Combust.*, Cambridge Monographs on Mechanics, Cambridge, UK: Cambridge University Press.

Poinsot, T. and Veynante, D., (2011) *Theoretical and Numerical Combustion*, 3 ed., Paris, France: CNRS.

Poinsot, T.J., Haworth, D.C., and Bruneaux, G., (1993) Direct Simulation and Modeling of Flame-Wall Interaction for Premixed Turbulent Combustion, *Combust. Flame*, **95**(1), pp. 118–132.

Ponizy, B., Claverie, A., and Veyssière, B., (2014) Tulip flame—The Mechanism of Flame Front Inversion, *Combust. Flame*, **161**(12), pp. 3051–3062.

Rumble, J.R., (2018) *CRC Handbook of Chemistry and Physics: A Ready-Reference Book of Chemical and Physical Data*, 99th ed., Boca Raton, FL: CRC Press.

Sackheim, R.L. and Masse, R.K., (2014) Green Propulsion Advancement: Challenging the Maturity of Monopropellant Hydrazine, *J. Propuls. Power*, **30**(2), pp. 265–276.

Smith, G.P., Golden, D.M., Frenklach, M., Moriarty, N.W., Eiteneer, B., Goldenberg, M., Bowman, C.T., Hanson, R.K., Song, S., Gardiner, W.C., Lissianski, V.V., and Qui, Z., (2016) GRI-Mech 3.0, available from http://www.me.berkeley.edu/gri_mech/.

Spalding, D.B., (1957) A Theory of Inflammability Limits and Flame-Quenching, *Proc. of the Royal Society of London, Ser. A: Mathematical, Physical and Engineering Sciences*, **240**(1220), pp. 83–100.

Turns, S.R., (2000) *An Introduction to Combustion: Concepts and Applications*, 2nd ed., McGraw-Hill Series in Mechanical Engineering, 2nd ed., Boston, MA: McGraw-Hill and WCB/McGraw-Hill.

Werling, L., Bätz, P., Ciezki, H., and Schlechtriem, S., (2018) Influence of Combustion Chamber Size (L*) on Characteristic Exhaust Velocity (C*) for a N_2O/C_2H_4 Premixed Green Propellant, in *Space Propulsion Conf.* Sevilla, Spain, 2018.

Werling, L., Hassler, M., Lauck, F., Ciezki, H.K., and Schlechtriem, S., (2017a) Experimental Performance Analysis (c* & c* Efficiency) of a Premixed Green Propellant Consisting of N_2O and C_2H_4, in *Proc. of 53rd AIAA/SAE/ASEE Joint Propulsion Conf.*, Atlanta, GA, USA, July 10–12, 2017.

Werling, L., Lauck, F., Freudenmann, D., Röcke, N., Ciezki, H., and Schlechtriem, S., (2017b) Experimental Investigation of the Flame Propagation and Flashback Behavior of a Green Propellant Consisting of N2O and C2H4, *J. Energy Power Eng.*, **11**(12), pp. 735–752.

Wichman, I.S. and Bruneaux, G., (1995) Head-On Quenching of a Premixed Flame by a Cold Wall, *Combust. Flame*, **103**(4), pp. 296–310.

Wilhelm, M., Negri, M., Hendrich, C., Wingborg, N., Gediminas, L., Adelö, L., Maleix, C., Chabernaud, P., Brahmi, R., Beauchet, R., Batonneau, Y.X., Kappenstein, C., Koopmans, R.J., Schuh, S., Bartok, T., Scharlemann, C.A., Anflo, K., Persson, M., Dingertz, W., and Gotzig, U., (2017) The RHEFORM Project—Developments for ADN-Based Liquid Monopropellant Thrusters, in *Proc. of 53rd AIAA/SAE/ASEE Joint Propulsion Conf.*, Atlanta, GA, USA, July 10–12, 2017.

Xiao, H., (2016) *Experimental and Numerical Study of Dynamics of Premixed Hydrogen-Air Flames Propagating in Ducts*, Springer Theses, Berlin-Heidelberg, Germany: Springer-Verlag.

Xiao, H., Houim, R.W., and Oran, E.S., (2015) Formation and Evolution of Distorted Tulip Flames, *Combust. Flame*, **162**(11), pp. 4084–4101.

Zimont, V.L., (2016) Damköhler-Shelkin Paradox in the Theory of Turbulent Flame Propagation, and a

Concept of the Premixed Flame at the Intermediate Asymptotic Stage, *Flow Turbulence Combust.*, **97**(3), pp. 875–912.